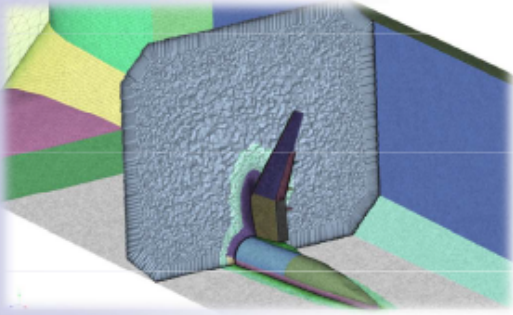


TASによるCRM-HLの風洞壁を考慮したRANS定常空力解析・田中 健太郎 (菱友システムズ),
伊藤 靖, 村山 光宏 (JAXA), 古谷 龍太郎 (菱友システムズ)

July 12, 2023
Ninth Aerodynamics Prediction Challenge (APC-9)
1A03

Reynolds-averaged Navier-Stokes simulations of CRM-HL in wind tunnel using TAS code

TASによるCRM-HLの風洞壁を考慮したRANS定常空力解析



○Kentaro TANAKA (Ryoyu Systems)
Yasushi ITO (JAXA)
Mitsuhiro MURAYAMA (JAXA)
Ryutaro FURUYA (Ryoyu Systems)

Cases calculated

2

■ Test Cases

- Case 1: Turbulence model verification study in 2D simulations
- Case 2: $C_{L,max}$ study "in-tunnel" simulations

	Case 1	(ref.) Case 1 of APC-8 "free-air"	Case 2 "in-tunnel"
Geometry	2D CRM-HL	3D CRM-HL	3D CRM-HL + QinetiQ 5m WT
Flap deflection (inboard/outboard)	—	40°/37°	
AoA	16°	(2.78°) 7.05° (11.29°) 17.05° 19.57° 21.47°	5.98° (9.98°) 15.48° 17.98° 19.98°
α_c: collected α_u: uncollected			
Initial conditions	cold starts	warm & cold starts	warm starts
Grid	Family 1 ^{*1}	240-JAXA-unstructured ^{*3}	240-JAXA-unstructured + wind tunnel walls
Grid Level	L1~7 ^{*2}	C-level ^{*4} ~86Mpts	C-level ~122Mpts

*1 Grid provided by NASA TMR

*2 L1 (coarsest) to L7 (finest)

*3 Grid provided by JAXA (downloadable from HLPW-4 website)

*4 A-level (coarsest) to D-level (finest)

Computational conditions & Numerical methods

3

Computational conditions

- Case1
 - Mach = 0.2, Re = 5.00×10^6 ($C_{ref} = 1$), $T_{ref} = 272.1K$
- Case2
 - Mach = 0.2, Re = 5.49×10^6 ($C_{ref} = 275.8$ in), $T_{ref} = 521R$ (289.4K)

Numerical methods

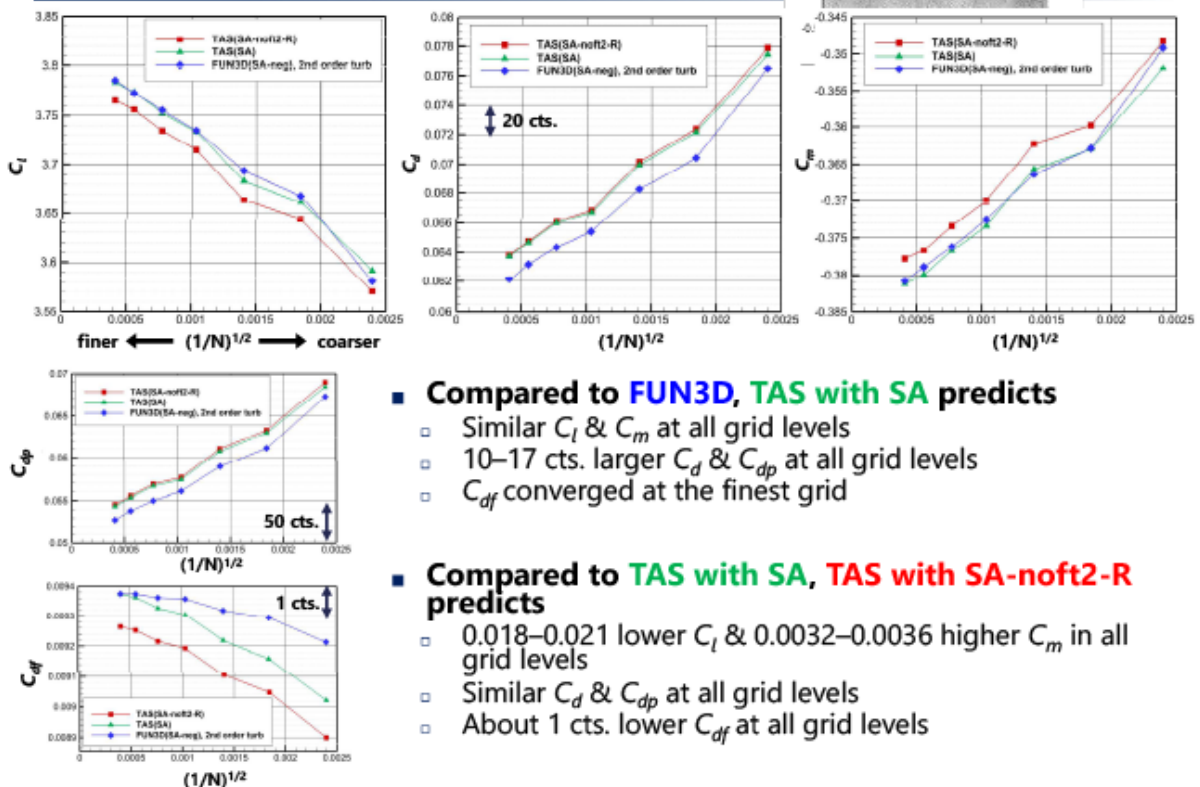
Code	TAS
Governing Equations	RANS (Reynolds Averaged Navier-Stokes) Eq.
Discretization	Cell-vertex finite volume method
Convection term	HLLEW (Harten-Lax-vanLeer-Einfeldt-Wada)
Reconstruction method	2 nd order Unstructured MUSCL
Time integration	LU-SGS implicit
Turbulence model (fully turbulent)	SA-noft2-R ($C_{rot}=1$) SA for Case 1

Computational Resources

- JAXA Supercomputer System generation 3 (JSS3) was used for these computations.



Aerodynamic coefficients (Case 1)



Compared to FUN3D, TAS with SA predicts

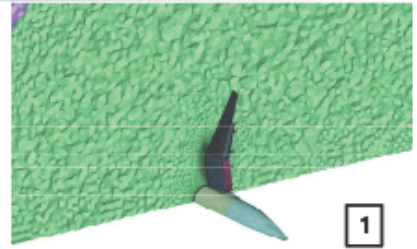
- Similar C_l & C_m at all grid levels
- 10–17 cts. larger C_d & C_{dp} at all grid levels
- C_{df} converged at the finest grid

Compared to TAS with SA, TAS with SA-noft2-R predicts

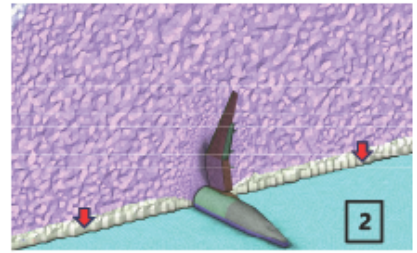
- 0.018–0.021 lower C_l & 0.0032–0.0036 higher C_m in all grid levels
- Similar C_d & C_{dp} at all grid levels
- About 1 cts. lower C_{df} at all grid levels

Grid generation & initial conditions in-tunnel simulations 5

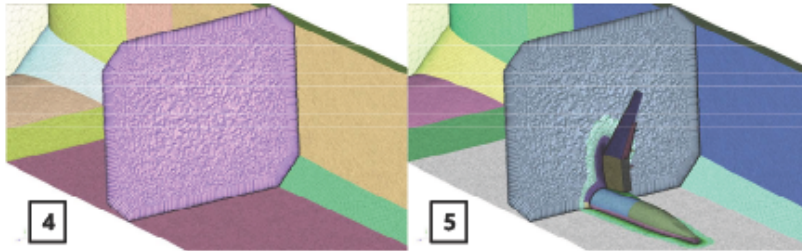
1. Prepared the free-air (APC-8) grid & results.
2. Replaced the symmetry plane with a tunnel floor and standoff.
 - Automatic local remeshing features of MEGG3D were used.
 - Flow variables were extrapolated by 0th order.
3. Extracted grid elements & solution data at a specified distance from the CRM-HL (< 0.3 MAC) to obtain element-independent results as much as possible from in-tunnel simulations.
4. Prepared an empty-tunnel grid separately.
 - Convergence results were calculated using estimated back pressure.
5. Installed #3 in #4 at each angle of attack.
 - Automatic local remeshing features of MEGG3D were used.
 - Velocity vectors were rotated with angle of attack within the free-air grid region.
 - Warm start from the $\alpha = 7.05^\circ$ result of the free-air simulation were conducted in all in-tunnel calculations.
 - Flow variables were substituted from the empty-tunnel results within the in-tunnel grid & remeshed region.



1

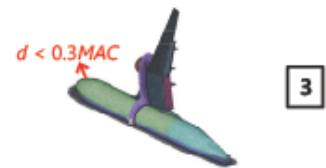


2



4

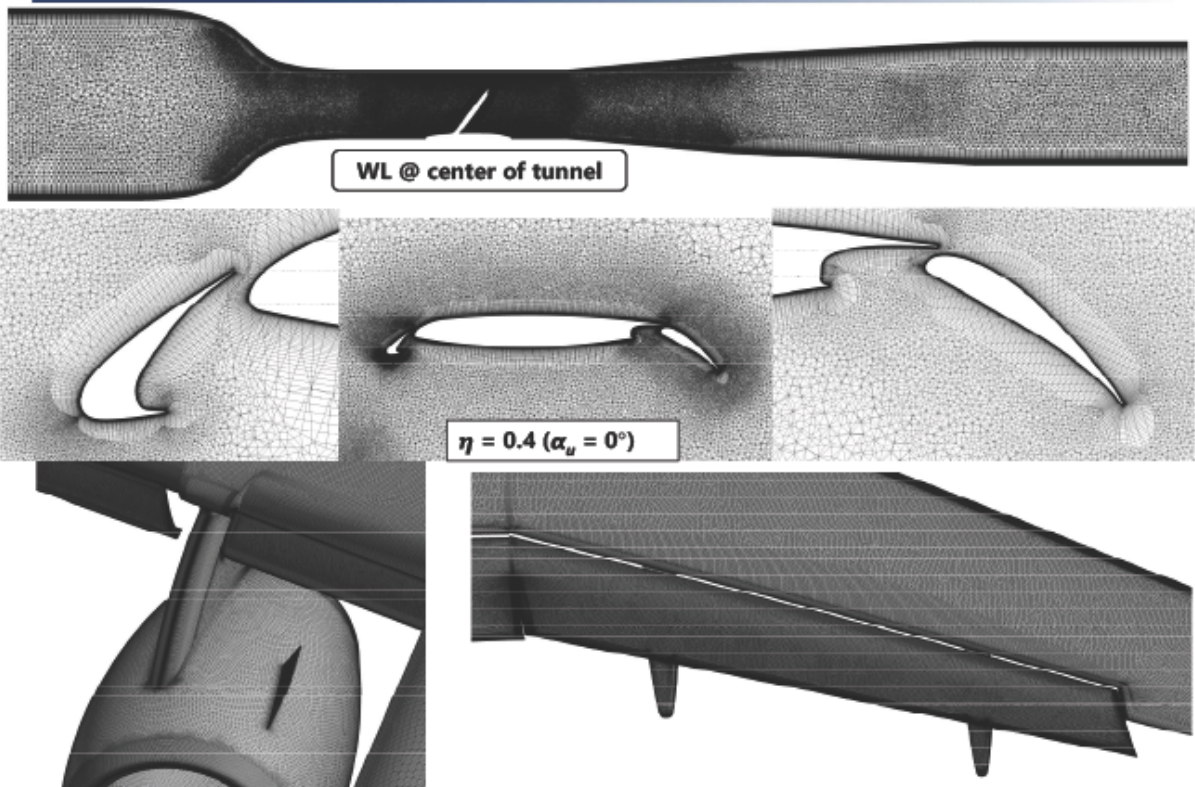
5



3

* Same procedure as previous research during HiLiftPW-3, doi: 10.2514/1.C036741

Sectional & surface grids 6



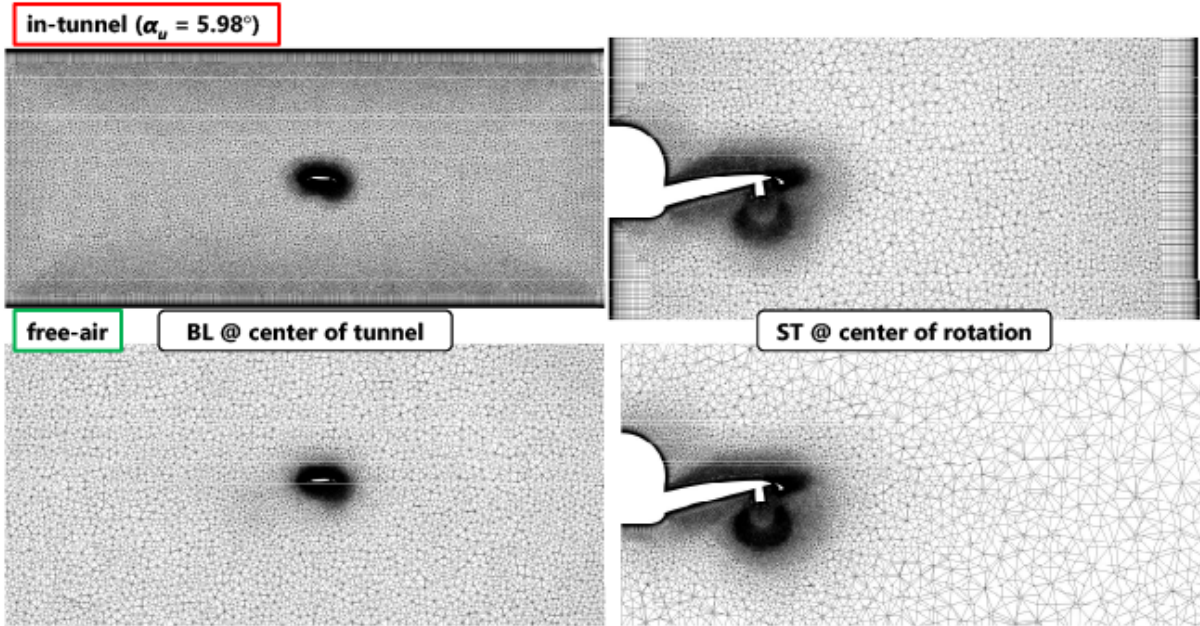
WL @ center of tunnel

$\eta = 0.4 (\alpha_u = 0^\circ)$

Comparison of sectional grids

7

- Both grids had the same elements around the CRM-HL (< 0.3 MAC).
- Spatial grid resolutions of **in-tunnel** grids were finer than the **free-air** grid.



Boundary conditions & reference Mach number

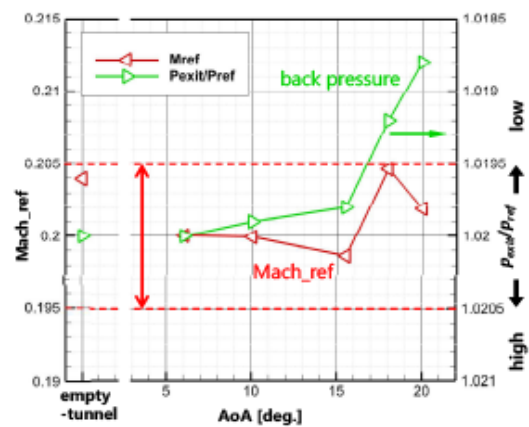
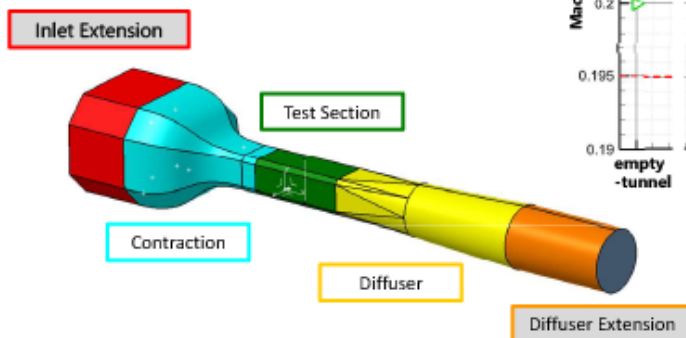
8

Mach_ref

- Calculated by the static pressure drop through the nozzle (as specified).
- Calculated values were within a desired tolerance (0.195–0.205) by adjusting back pressure.

Inflow

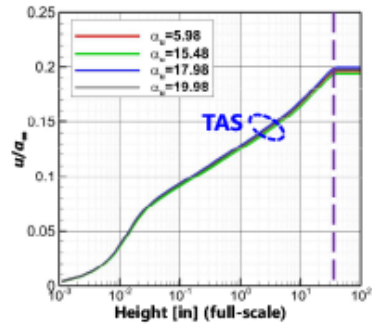
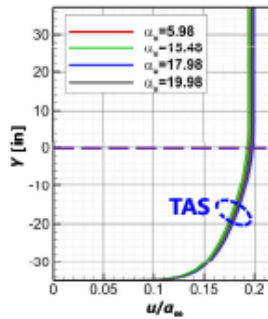
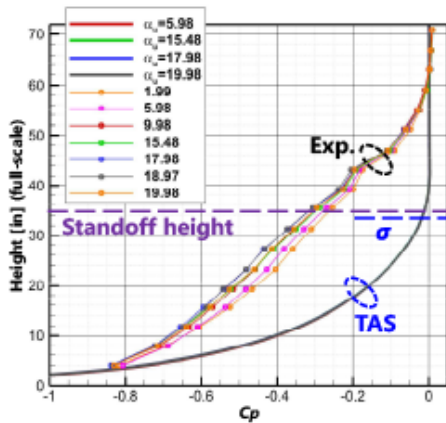
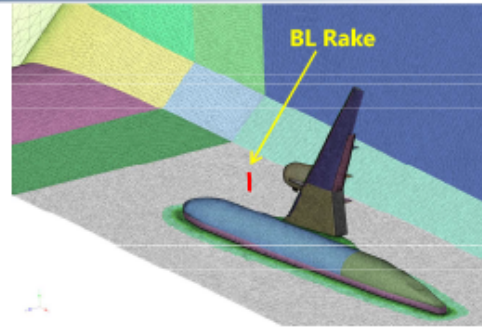
- $\frac{P_T}{P_\infty} = \left(1 + \frac{\gamma-1}{2} M^2\right)^{\frac{\gamma}{\gamma-1}}$
- $\frac{T_T}{T_\infty} = 1 + \frac{\gamma-1}{2} M^2$



Boundary layer profile at the tunnel floor

9

- **TAS results disagree with exp.**
 - Similar tendencies have been reported*1 at HLPW-4
 - The results in the experiment appear to have been laminar.
- **TAS results seem correct if the boundary layer is turbulent.**
 - Boundary layer thickness ($\sigma \sim 33.5$ in) is close to standoff height (= 35 in).

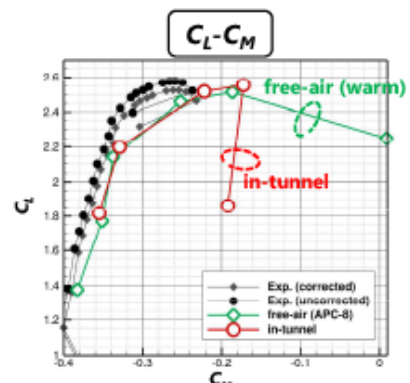
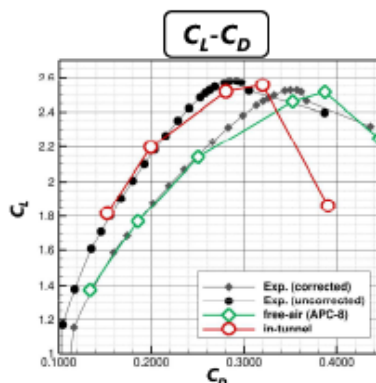
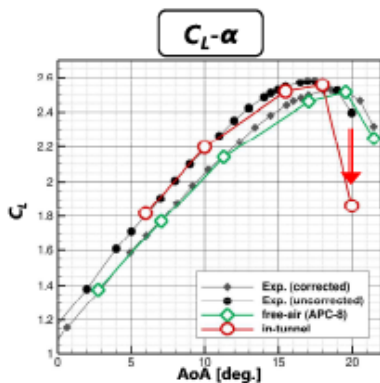


*1 https://hllftpw.larc.nasa.gov/Workshop4/WorkshopPresentations/07_GMGW3_HLPW4_WMLES-LB.pdf

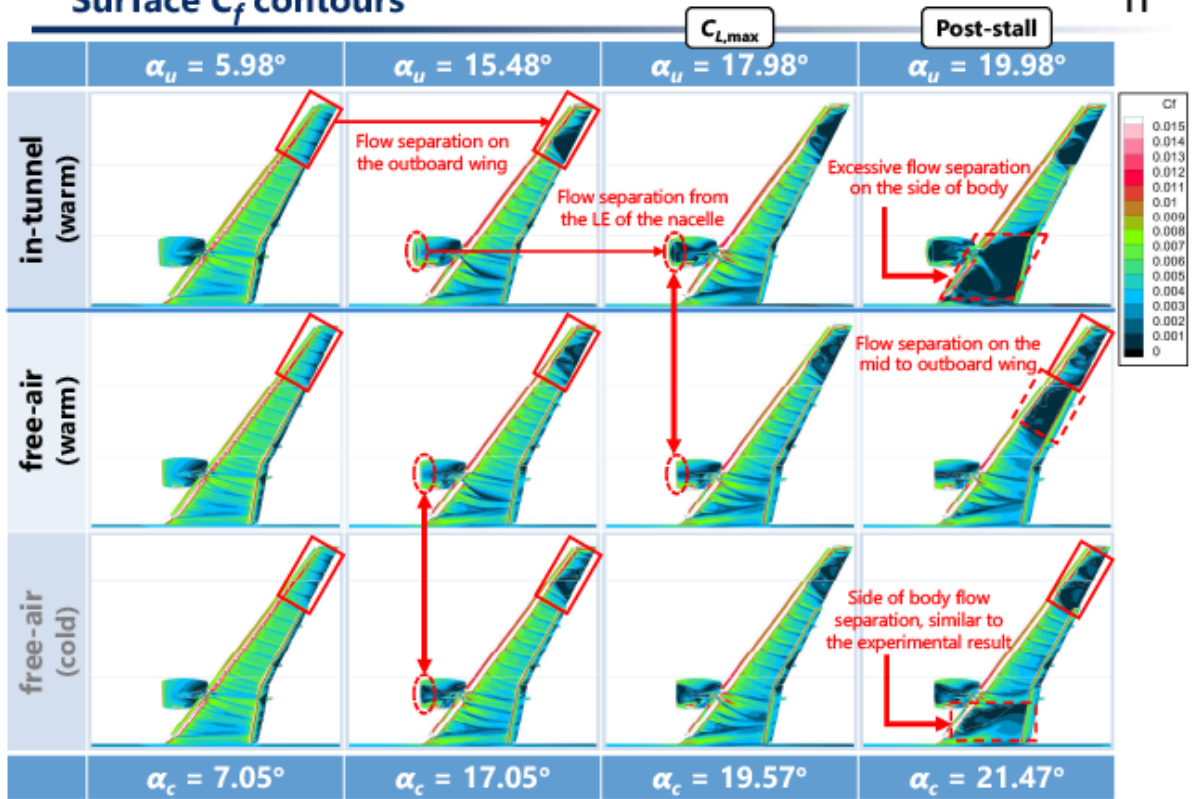
Aerodynamic coefficients (Case 2)

10

- **As for results of in-tunnel simulations,**
 - C_L agrees well with exp. except a large drop at the post-stall.
 - Near $C_{L,max}$, C_L is slightly lower and C_D is slightly higher than exp.
 - C_m tends to be higher (=pitch-up) than exp. throughout the AoA.

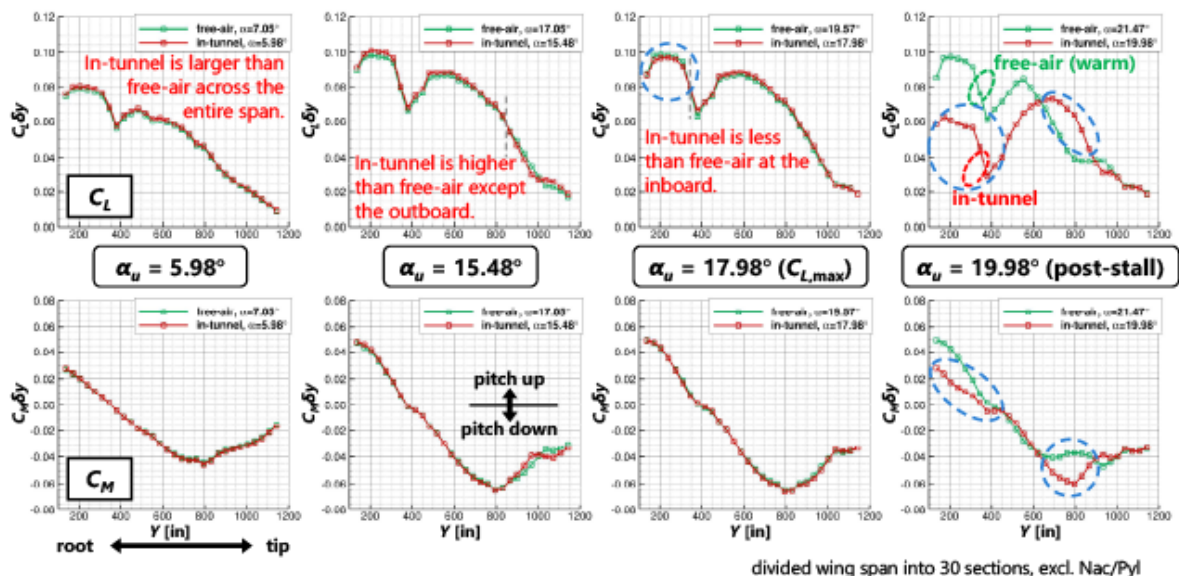
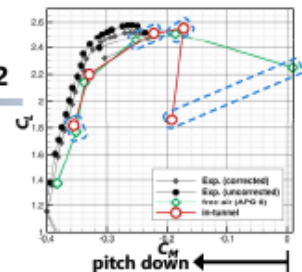


Surface C_f contours



Spanwise sectional C_l & C_m distributions

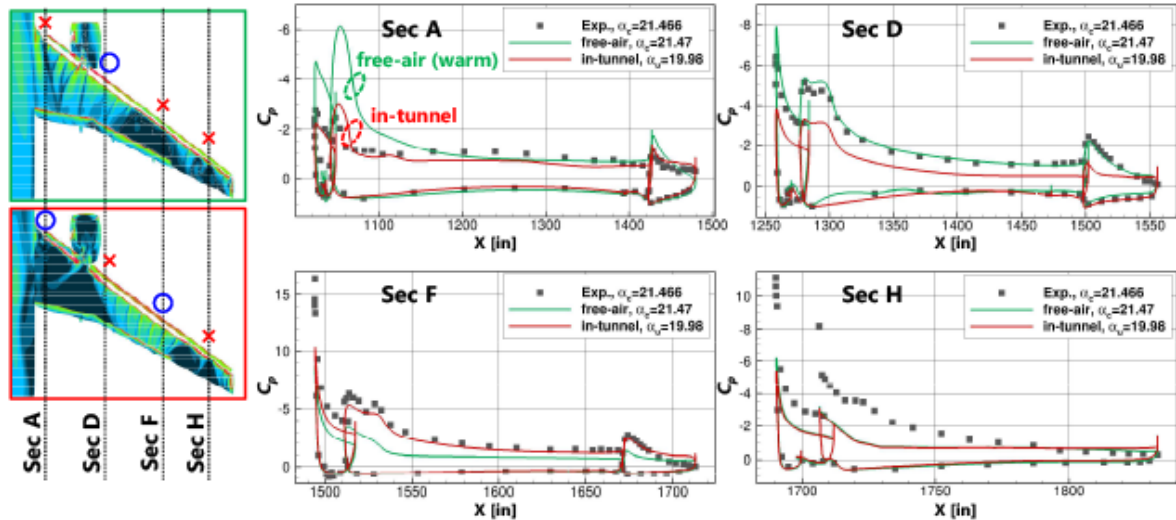
- Compared to the corresponding free-air results, the inboard lift of **in-tunnel** results is higher at $\alpha_u \leq 15.48^\circ$ because of the effect of the standoff, and lower at $\alpha_u \geq 17.98^\circ$ because of the floor boundary layer to be discussed.
- The pitch-down trend at the post-stall in the **in-tunnel** result is due to the excessive side of body separation and attached flow on the midspan.



divided wing span into 30 sections, excl. Nac/Pyl

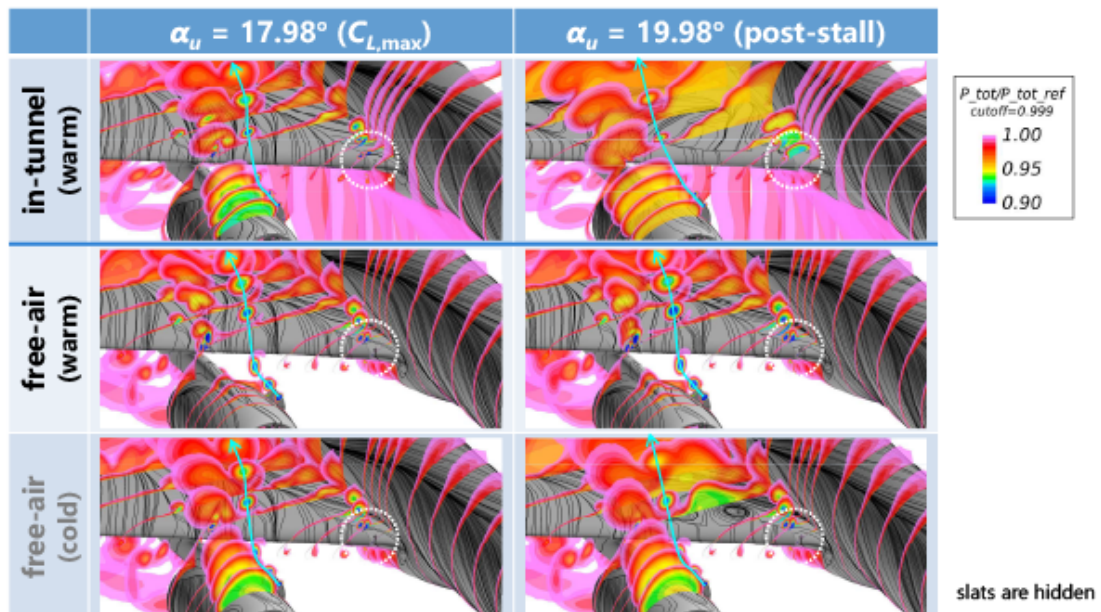
Spanwise sectional C_p distribution at $\alpha_U = 19.98^\circ$ (post-stall) 13

- In sec A, **in-tunnel** result is closer to that of the experiment, and the **free-air** result shows a higher suction peak due to the attached flow.
- In sec D, **free-air** result is closer to that of the experiment because the **in-tunnel** result has excessive separation near this section.
- In sec F, **in-tunnel** result is closer to that of the experiment because the **free-air** result has large separation at the wake of slat brackets on the outboard wing.
- In sec H, both results disagree with that of the experiment due to large flow separation at the wake of slat brackets.



Surface streamlines & sectional total pressure distribution 14

- Compared to free-air cases, **in-tunnel** cases show thicker boundary layers on the LE of the wing root because of the boundary layer developed on the tunnel floor.
 - The thicker boundary layer may have contributed to the excessive side of body separation in the post-stall case.



Summary

15

■ Turbulence model study in 2D simulation

- SA in TAS code were verified by comparison with FUN3D results.
- Compared to SA in TAS code, SA-noft2-R($C_{rot}=1$) shows
 - Lower C_l , C_{df} and higher C_m
 - Similar C_d and C_{dp}

■ $C_{L,max}$ study

- As for results of **in-tunnel** simulations,
 - Aerodynamic characteristics showed good agreement with exp. until $C_{L,max}$.
 - Near $C_{L,max}$ flow separations occurred on the wake of slat brackets on the outboard wing and nacelle lip.
 - The side of body separation seen in the experiment was observed, but overpredicted at the post-stall.
 - This appeared to be the result of the thicker boundary layer on the LE of the wing root because of the boundary layer developed on the tunnel floor.